Cytotherapy 000 (2020) 1–13

Contents lists available at ScienceDirect

CYTOTHERAPY

journal homepage: www.isct-cytotherapy.org

Mesenchymal stem/stromal cells stably transduced with an inhibitor of CC chemokine ligand 2 ameliorate bronchopulmonary dysplasia and pulmonary hypertension

Toshihiko Suzuki[1,2], Yoshiaki Sato[1,*], Hidenori Yamamoto[2], Taichi Kato[2], Yuma Kitase[1,2], Kazuto Ueda[1,2], Haruka Mimatsu[1,2], Yuichiro Sugiyama[1], Atsuto Onoda[1,3,4], Shigeki Saito[5], Yoshiyuki Takahashi[2], Takayuki Nakayama[6], Masahiro Hayakawa[1]

[1] *Division of Neonatology, Center for Maternal-Neonatal Care, Nagoya University Hospital, Nagoya, Japan*
[2] *Department of Pediatrics, Nagoya University Graduate School of Medicine, Nagoya, Japan*
[3] *Faculty of Pharmaceutical Sciences, Sanyo-Onoda City University, Yamaguchi, Japan*
[4] *Research Fellow of Japan Society for the Promotion of Science, Tokyo, Japan*
[5] *Department of Hematology and Oncology, Japanese Red Cross Nagoya Daini Hospital, Nagoya, Japan*
[6] *Department of Transfusion Medicine, Aichi Medical University, Nagakute, Japan*

ARTICLE INFO

Article History:
Received 10 October 2019
Accepted 22 January 2020
Available online xxx

Keywords:
7ND
mesenchymal stem/stromal cell
perinatal bronchopulmonary dysplasia
pulmonary hypertension

ABSTRACT

Perinatal bronchopulmonary dysplasia (BPD) is defined as lung injury in preterm infants caused by various factors, resulting in serious respiratory dysfunction and high mortality. The administration of mesenchymal stem/stromal cells (MSCs) to treat/prevent BPD has proven to have certain therapeutic effects. However, MSCs can only weakly regulate macrophage function, which is strongly involved in the development of BPD. 7ND-MSCs are MSCs transfected with 7ND, a truncated version of CC chemokine ligand 2 (CCL2) that promotes macrophage activation, using a lentiviral vector. In the present study, we show in a BPD rat model that 7ND-MSC administration, but not MSCs alone, ameliorated the impaired alveolarization evaluated by volume density and surface area in the lung tissue, as well as pulmonary artery remodeling and pulmonary hypertension induced by BPD. In addition, 7ND-MSCs, but not MSCs alone, reduced M1 macrophages and the messenger RNA expressions of interleukin-6 and CCL2 in the lung tissue. Thus, the present study showed the treatment effect of 7ND-MSCs in a BPD rat model, which was more effective than that of MSCs alone.

Introduction

Neonatal bronchopulmonary dysplasia (BPD) is a lung injury caused by various factors, such as intrauterine inflammation, surfactant deficiency, mechanical trauma and oxygen toxicity [1]. Although perinatal/neonatal medicine has been developing recently, BPD is still one of the major causes of mortality in preterm infants [2,3]. In addition, BPD causes pulmonary hypertension (PH) and long-term respiratory and/or neurodevelopmental complications. Current advanced respiratory management and drug treatment are somewhat effective for BPD [4,5], but not enough [6]. Therefore, the development of a novel treatment for BPD is an urgent task in neonatal medical care.

Mesenchymal stem/stromal cells (MSCs) are widely used as stem cell sources to develop a novel stem cell therapy for various diseases [7–10]. As for BPD, some animal studies using MSCs have shown the treatment effect of MSC administration to some degree [11–15]. However, an important pathogenic factor in BPD is lung tissue disorder due to macrophages [16]. MSCs can modulate T-cell, B-cell, natural killer cell and dendritic cell functions, but not specifically macrophage function [17–20]. Therefore, a higher therapeutic effect on lung disorder can be possibly obtained when using MSCs with enhanced capability to suppress the activation/recruitment of macrophages.

One possible strategy to control macrophages is by using “7ND” [21,22]. The 7ND recombinant protein is a mutant of human CC chemokine ligand 2 (CCL2) protein lacking 2 to 8 N-terminal amino acids that functions as a potent antagonist of CC chemokine receptor type 2 (CCR2) [23]. CCL2 is a chemotactic factor for monocytes and also plays a role as a monocyte-activating factor, such as enhanced release of active oxygen and lysosomal enzyme and interleukin (IL)-6 production. Therefore, inhibiting CCL2 using 7ND can lead to the suppression of activation/recruitment of macrophages and then the improvement of lung tissue disorder. Furthermore, PH, an important complication of BPD, is caused by pulmonary angiogenesis and

* Correspondence: **Yoshiaki Sato**, MD, PhD, Division of Neonatology, Center for Maternal-Neonatal Care, Nagoya University Hospital, 65 Tsurumai-cho Showa-ku, Nagoya, 466-8550, Japan.
E-mail address: yoshiaki@med.nagoya-u.ac.jp (Y. Sato).

https://doi.org/10.1016/j.jcyt.2020.01.009

remodeling, which is promoted by inflammatory cells and cytokines [24–26]. The suppression of macrophages and inflammatory cytokines by 7ND can also be expected for the amelioration of the PH development.

In the present study, we hypothesized that 7ND-MSCs not only have a treatment effect by MSCs, but also weaken the negative effect of macrophages in BPD, showing superiority relative to MSCs. To confirm this hypothesis, we evaluated the therapeutic effects after intravenous administration of 7ND-MSCs in hyperoxia-induced BPD model rats.

Methods

Cell preparation of 7ND-MSCs

Rat MSCs were obtained from Wistar/ST rats as described elsewhere [27]. Gene transduction of a deletion mutant of human CCL2 (7ND) into MSCs was performed by using a lentiviral vector [28]. Briefly, 7ND was recloned from the 7ND pCDNA3 expression vector [22] into a lentiviral vector (pBGJR-EGFP; a gift from Dr. Stefano Rivella, Cornell University, New York, NY, USA) by using unique NheI and XbaI sites. An empty pBGJR-EGFP vector was used as a control. We produced vector stocks by transient transfection of 293T cells. The envelope-encoding plasmid pLP/VSVG, the packaging plasmid pCMV-dR8.91 and pBGJR-EGFP-7ND or empty pBGJR-EGFP were transfected into 293T cells using Lipofectamine 2000 (Invitrogen, Carlsbad, CA, USA). After 48 h, culture supernatant was collected and filtered through a 45-μm membrane filter. Rat MSCs were plated in Opti-MEM medium (GIBCO-BRL/Invitrogen, Carlsbad, CA, USA) onto 6-well plates at 1.0×10^5 cells per well and then incubated with vector stocks in the presence of Polybrene at 4 μg/mL (Sigma-Aldrich, St. Louis, MO, USA). After 8-h incubation, the medium was replaced with minimal essential medium (MEM) alpha (Invitrogen) containing 10% fetal bovine serum (Thermo Fisher Scientific, Waltham, MA, USA) and used after passage 5 to 15 (Figure 1A). The transduction efficiency was evaluated by counting green fluorescent protein (GFP)–positive cells with fluorescence-activated cell sorting.

Quantification of secreted 7ND

7ND-MSCs or control MSCs were seeded at a density of 2×10^2 cells per well in a 96-well plate. Culture supernatants were collected

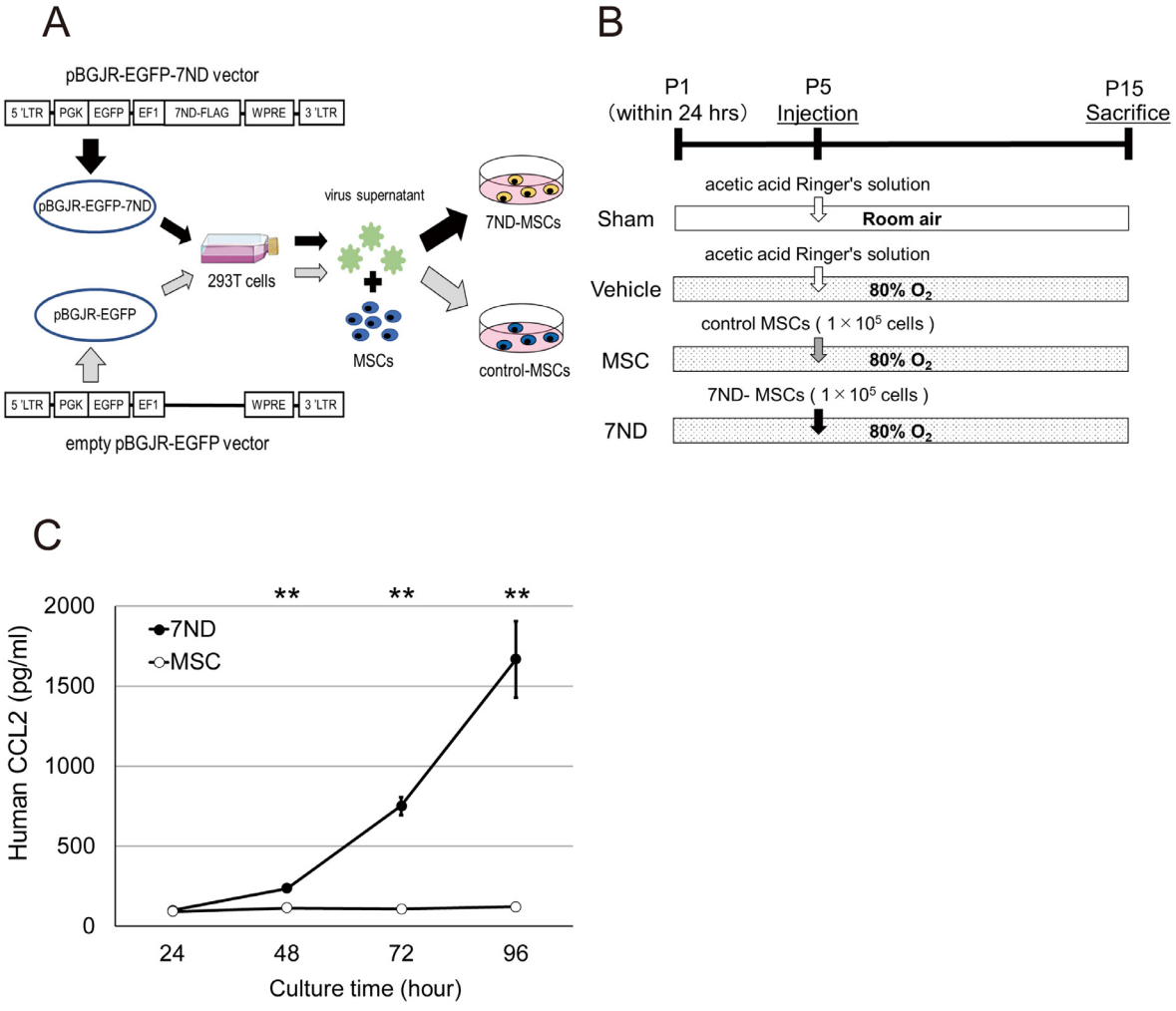

Figure 1. Experimental design and characterization of 7ND-MSCs. (A) Cell preparation of 7ND-MSCs and control MSCs. Gene transduction of a deletion mutant of human CCL2 (7ND) into MSCs was performed by using a lentiviral vector (pBGJR-EGFP). An empty pBGJR-EGFP vector was used as a control. Vector stocks were produced by transient transfection of 293T. MSCs were incubated with vector stocks in the presence of polybrene. Black and gray arrows indicate the flow of cell preparation of 7ND-MSCs and control MSCs, respectively. EF1, elongation factor-1 promoter; LTR, long terminal repeat; PGK, phosphoglycerate kinase promoter; WPRE, woodchuck hepatitis virus post-transcriptional regulatory element. (B) Schematic outline of the experimental protocol. Rat pups were exposed to room air (21% O_2) or 80% O_2 from birth to P15. At P5, 7ND-MSCs, control MSCs or vehicle (acetic acid Ringer's solution) was administered intravenously. P, postnatal day. (C) Quantification of human 7ND secreted from 7ND-MSCs and control MSCs. The 7ND content in culture supernatants of 7ND-MSCs (closed circle) and control MSCs (opened circle) collected for 4 days every 24 h was measured using a specific human CCL2 enzyme-linked immunosorbent assay. Data represent the mean ± SEM of five replicates. $^{**}P < 0.01$.

for 4 days every 24 h. Because 7ND was a deletion mutant of human CCL2, the 7ND content was measured using a specific human CCL2 enzyme-linked immunosorbent assay (ELISA) kit (Human CCL2 [MCP-1] ELISA Ready-SET-Go!, catalog number 88-7399, eBioscience Inc., San Diego, CA, USA), which recognizes human CCL2 but not rat CCL2. 7ND purified from the culture supernatants possesses inhibitory effects on macrophage migration induced by CCL2 [28].

Animal models and experimental protocol

All animal experimental protocols used in the present study were approved by the Institutional Review Board of Animal Experimentation of the Nagoya University School of Medicine (Nagoya, Japan; Protocol Numbers 27190 and 28215). Wistar/ST rat pups were exposed to normoxia (21% oxygen) or hyperoxia (80% O_2) from birth to postnatal day 15 (P15). At P5, 7ND-MSCs (1×10^5 cells), control MSCs (1×10^5 cells) in 0.1 mL acetic acid Ringer's solution or vehicle (only 0.1 mL acetic acid Ringer's solution) were administered via the right external jugular vein. The newborn rat pups were divided into the following four groups: sham group, room air + vehicle; vehicle group, hyperoxia + vehicle; MSC group, hyperoxia + control MSCs; and 7ND group, hyperoxia + 7ND-MSCs.

All rats were maintained under a 12-h light/dark cycle. To prevent oxygen toxicity, the nursing mother rats were rotated once every 2 days between the litters in the normoxia and hyperoxia groups. The survival rate and body weight of the pups of each group were evaluated once every 2 days throughout the experiments. All rats were humanely killed at P15 to evaluate the treatment effect (Figure 1B).

Tissue preparation

The rats were humanely killed after transcardiac perfusion with saline at P15 under deep anesthesia with pentobarbital intraperitoneal injection, and the lungs were inflated with 4% paraformaldehyde via a tracheal catheter at 20-cmH_2O pressure for 20 min, followed by immersion–fixation in 4% paraformaldehyde overnight at 4°C. Subsequently, the right lower lungs were immersed in a sucrose solution for at least 2 days and embedded in Tissue-Tek O.C.T. Compound (Sakura Finetek, Tokyo, Japan) for subsequent preparation of 10-μm frozen sections. The left lungs, after immersion–fixation in 4% paraformaldehyde, were dehydrated with a graded series of ethanol and xylene, embedded in paraffin and cut into 5-μm axial sections.

Tissue morphometry

Paraffin sections were deparaffinized and stained with hematoxylin and eosin (H-E) for histology and morphometry. The extent of the alveolar maldevelopment was determined using tissue volume density(VD_T), mean linear intercept (L_m) and alveolar surface area (S_A) in the left lungs. The VD_T was expressed as the proportion of lung tissue (alveolar ducts and sacs) in the lungs as previously described [29]. The VD_T was counted using a 10 × 10 grid with 100 evenly spaced points, 25 μm apart, in each of three random fields of six sections (50 μm apart; total of 18 fields). The L_m was provided as previously described with minor modifications [30]. Random images were obtained with 40 × fields and viewed equally at ten-spaced horizontal lines, 25-μm long. Subsequently, the distance from the first airspace wall intersecting each horizontal line to an adjacent airspace wall was measured. The image was obtained in each of five random fields of six sections. The S_A was calculated based on the following formula: $S_A = 4 \times VD_T \times$ lung volume/L_m [31]. Volumetric assessment using the left lung was performed to assess lung volume. At P14, chest computed tomography (CT) scan was performed using an *in vivo* micro-CT scanner (Skyscan 1176; Bruker, Kontich, Belgium) with a 12.85-μm voxel size and the following conditions: 45 kVp, 556 uA, 43-ms exposure, rotation step 0.700°, frame averaging 2, with a 180° angular range. For *in vivo* lung micro-CT scan acquisition, pups were anesthetized with 1.5–2.5% isoflurane. Datasets were reconstructed using a software program (NRecon; Bruker). Volumetric analysis of CT images was performed using the SkyScan CT-analyzer program (CTAn, ver.1.13; Bruker). Briefly, the boundary of each left lung on CT was identified and outlined manually, excluding the heart, the central airways and the major blood vessels. Subsequently, a three-dimensional image was reconstructed, and the lung volume was automatically calculated.

Differential cell counts of blood and bronchoalveolar lavage fluid

Blood and bronchoalveolar lavage fluid (BALF) were collected at P15. After collecting blood, differential cell counts of the blood were performed using the fully automated differential hematology analyzer (VetScan HM5; Abaxis, Union City, CA, USA). Bronchoalveolar lavage was performed by instilling 0.6 mL (0.3 mL × 2) saline. BALF was stained with Türk solution, and the total cell number was counted using Burker chambers. Subsequently, a 100-μL aliquot was centrifuged and plated onto glass slides. Differential cell counts were made from centrifuged preparations stained with May-Giemsa staining, and at least 200 cells were counted in each animal [32,33].

Immunofluorescence staining

The following primary antibodies were used in immunofluorescence staining: rabbit anti-Ki67 (Abcam, Cambridge, United Kingdom; diluted to 1:100), rabbit anti-inducible nitric oxide synthase (iNOS; Abcam; diluted to 1:40), rabbit anti-CD206 (Abcam; diluted to 1:100), goat anti-ionized calcium binding adapter molecule-1 (Iba-1; Abcam; diluted to 1:1000) and mouse anti-α-smooth muscle actin (α-SMA; Sigma-Aldrich; diluted to 1:2000). The lung sections were immunostained as previously described [10] with minor modifications. Briefly, paraffin-embedded lung sections were deparaffinized in xylene and rehydrated through graded ethanol into phosphate-buffered saline (PBS). Antigen was retrieved by heating the sections for 10 min in 10-mmol/L citrate buffer (pH 6.0). The sections were blocked in PBS containing 0.1% Triton and 4% donkey serum and incubated overnight at 4°C with the respective primary antibodies. Subsequently, the lung sections were incubated with Alexa Fluor 488, Alexa Fluor 546, Alexa Fluor 555 and/or Alexa Fluor 647–labeled secondary antibodies (Invitrogen; diluted to 1:500) for 1 h at room temperature and mounted with ProLong Gold Antifade reagent containing 4′,6-diamidino-2-phenylindole (DAPI; Thermo Fisher Scientific).

Assessment of 7ND-MSC engraftment

To assess the engraftment of 7ND-MSCs and control MSCs, immunofluorescence staining for rabbit anti-GFP (Abcam; diluted to 1:1000) and DAPI nuclear staining were performed with 10-μm frozen sections in the same way as that described above for paraffin sections.

Assessment of lung inflammation

The polarity discrimination of macrophages in the lungs was performed with immunofluorescence staining for Iba-1, iNOS and CD206. Three random fields of 352 × 264 μm under 200 × magnification in two sections each were examined to count both Iba-1– and iNOS-positive cells as M1 macrophages, and Iba-1/CD206 double-positive cells as M2 macrophages.

Assessment of pulmonary artery remodeling

The degree of medial wall thickness (MWT) of the peripheral pulmonary vessels (<50 μm in diameter) was determined using lung tissue sections stained for α-SMA. MWT was measured by using the following formula: 2 MT/ED × 100, where MT is the distance between internal and external elastic laminae, and ED is the external diameter. For MWT assessment, random images containing 10 vessels were used on each of the two slides [34,35]. Sections stained for α-SMA and Ki-67, a nuclear proliferating marker, were used to assess vascular smooth muscle cell proliferation. The percentage of vessels with at least one Ki67-positive nucleus in the smooth muscle cells was determined in 10 vessels (<50 μm in diameter) on each of the two slides [36,37].

Assessment of PH

Dry weight ratio of the right ventricle (RV) to the left ventricle (LV) plus septum (S) (RV/LV+S) and right ventricular systolic pressure (RVSP) were measured at P15 to assess PH. The hearts were dissected to separate the RV from the LV+S. The dry weight was measured after placing in a drying oven at 60°C for 48 h, and the RV/LV+S ratio was calculated [38]. RVSP was measured percutaneously by inserting a 23-gage needle attached to a pressure transducer and an amplifier system (LEG-1000; Nihon Kohden Co, Tokyo, Japan) [39,40].

Real-time polymerase chain reaction of the lung tissue

RNA was extracted after homogenization of snap-frozen lungs of P15 rats using TriZol reagent (Life Technologies, Carlsbad, CA, USA) and quantified using Nanodrop spectroscopy (Thermo Fisher Scientific). Complementary DNA (cDNA) was synthesized using SuperScript VILO cDNA Synthesis Kit (Invitrogen). Quantitative real-time polymerase chain reaction (RT-PCR) was performed using Brilliant III Ultra-Fast SYBR Green QPCR Master Mix (Agilent Technologies, Santa Clara, CA, USA) on a Mx3005P RT QPCR System (Agilent Technologies) as follows: 3 min at 95°C and then 40 cycles of 10 s at 95°C and 22 s at 60°C. The primer sequences were as follows: IL-6 sense, CCACTTCACAAGTCGGAGGCTTA; antisense, GTGCATCATCGCTGTTCATACAATC; *CCL2* sense, CTATGCAGGTCTCTGTCACGCTTC; antisense, CAGCCGACTCATTGGGATCA; Glyceraldehyde-3-phosphate dehydrogenase (GAPDH) sense, GGCACAGTCAAGGCTGAGAATG; and antisense, ATGGTGGTGAAGACGCCAGTA [39].

Statistical analyses

Statistical analyzes were performed using JMP13.0 software (SAS Institute, Cary, NC, USA). Two-group analyses of quantification of human 7ND were compared using Student's *t*-test. The survival rate, determined using the Kaplan–Meier method, was calculated on day 15. Statistical comparisons among the four groups were performed using one-way analysis of variance, followed by post-hoc multiple comparisons using the Tukey method. All values were presented as the mean with standard error. Statistical significance was defined as $P < 0.05$.

Results

Quantification of human 7ND secreted from 7ND-MSCs

To confirm 7ND secretion, we cultured 7ND-MSCs or control MSCs and measured the 7ND content in the respective supernatant with a specific human CCL2 ELISA. 7ND-MSCs secreted a large amount of 7ND, whereas control MSCs did not (Figure 1C).

Survival rate and body weight gain

The survival rate after 15 days of hyperoxia exposure was 60.0%, 50.0% and 47.7% in the 7ND-MSC-treated (7ND), control MSC-treated (MSC) and vehicle-treated groups, respectively. No statistically significant difference was found among the three groups exposed to hyperoxia (Figure 2A). No significant difference was found in the body weight at P1 after birth and P5 with intravenous injection among the three groups exposed to hyperoxia. However, at P15, the body weight in the vehicle group was lower than that in the sham group (normoxia group), but it was higher in the 7ND group compared with the vehicle ($P < 0.01$) and control MSC groups ($P = 0.0567$) (n = 64 for sham, 44 for vehicle, 44 for MSC and 40 for 7ND; Figure 2B).

Impact of 7ND-MSCs on lung tissue

Immunofluorescence staining for GFP and DAPI nuclear staining of lung frozen sections was performed to detect 7ND-MSCs and control MSCs in lung tissue. Several GFP-positive cells were detected in the lung tissue (Figure 3A).

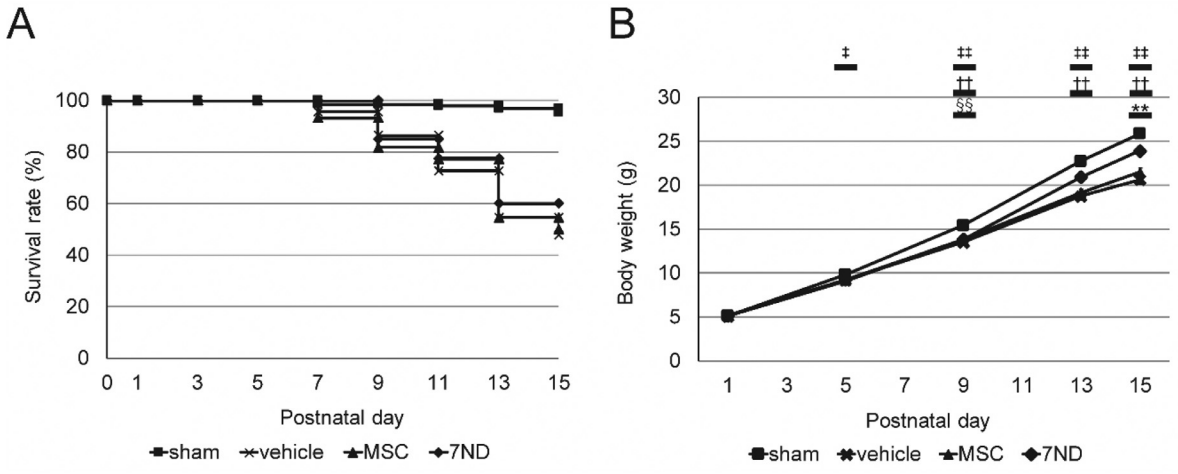

Figure 2. Survival rate and body weight gain. (A) Survival time course of each group from P0 to P15. The survival rate was not different among the three groups exposed to hyperoxia (vehicle, MSC and 7ND). (B) Postnatal change in body weight of pups from P0 to P15. The body weight at P15 in the 7ND-MSC–treated group was higher than that in the vehicle- and control MSC-treated groups. n = 64 for sham, 44 for vehicle, 44 for MSC and 40 for 7ND. $^{**}P < 0.01$, 7ND vs. vehicle; $^{\dagger\dagger}P < 0.01$, sham vs. vehicle; $\ddagger P < 0.05$ and $\ddagger\ddagger P < 0.01$, sham vs. MSC; §§$P < 0.01$, sham vs. 7ND.

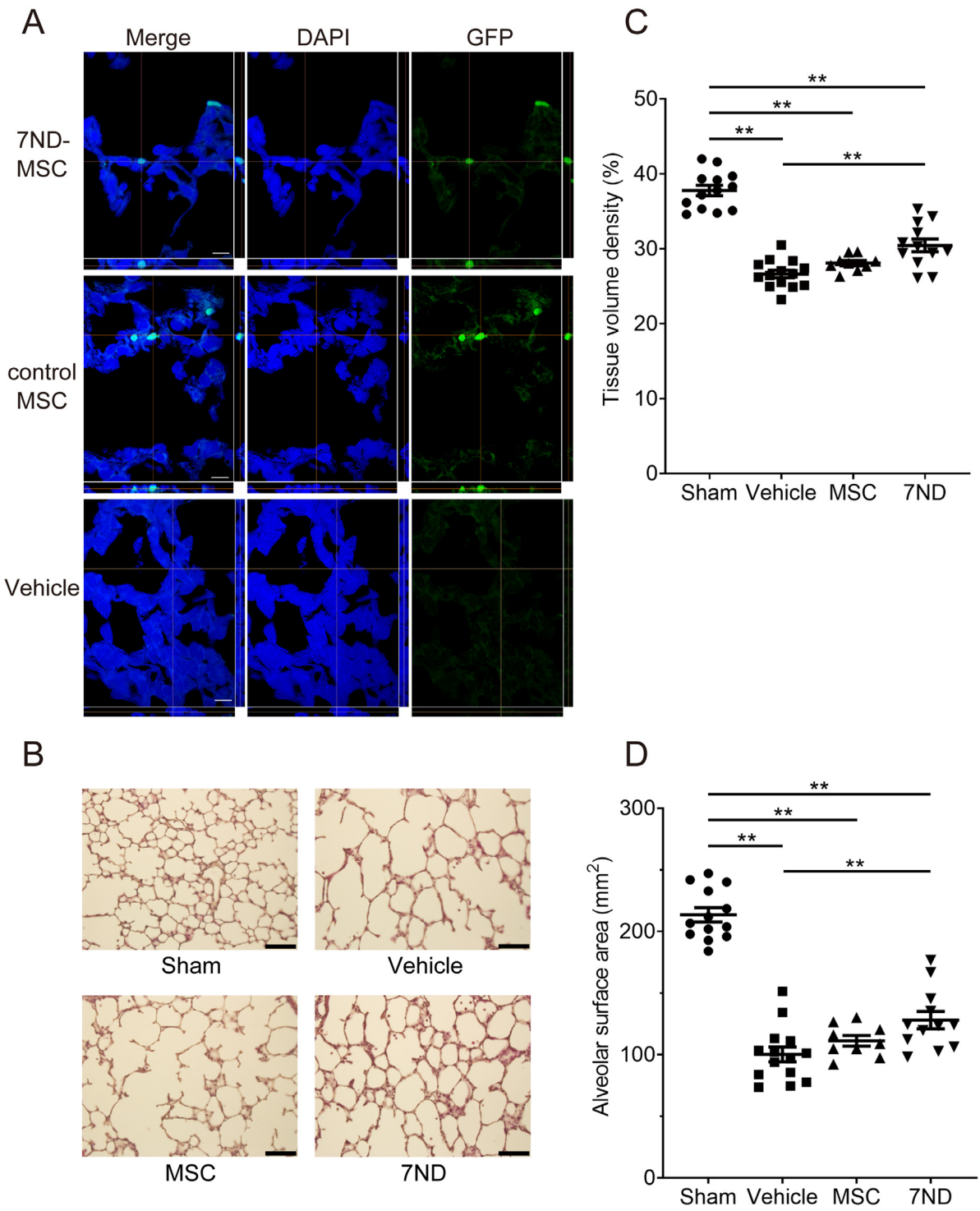

Figure 3. Impact of 7ND-MSCs on lung tissue. (A) Representative pictures of immunofluorescence staining for GFP and DAPI nuclear staining. Scale bars indicate 10 μm. (B) Representative lung tissue of each group with H-E staining. Scale bars indicate 100 μm. (C and D) VD_T and S_A at P15. VD_T and S_A of the 7ND-MSC–treated group were significantly lower than those of the vehicle-treated group, whereas the VD_T and S_A were not statistically different between the vehicle- and control MSC-treated groups. n = 13 for sham, 14 for vehicle, 9 for MSC and 12 for 7ND. $^{**}P < 0.01$.

Lung paraffin sections were stained with H-E to evaluate lung histology and morphometry. The lungs in the sham group showed normal alveolarization, whereas lungs exposed to 80% O_2 had alveolar size heterogeneity. Among the hyperoxia groups, only the lungs in the 7ND-MSC–treated group were significantly morphologically ameliorated compared with those of the vehicle and control MSC groups (Figure 3B). In the morphometric analyses, VD_T, L_m and S_A were measured, and the lung volume was assessed with chest CT (n = 13 for sham, 14 for vehicle, 9 for MSC and 12 for 7ND). The VD_T, which reflects the percentage of lung tissue in the lungs, in the vehicle group was significantly lower than that in the sham group, whereas the VD_T in the 7ND-MSC–treated group was significantly higher than that in the vehicle-treated group ($P < 0.01$; Figure 3C). No statistical difference was found in the L_m and lung volume among

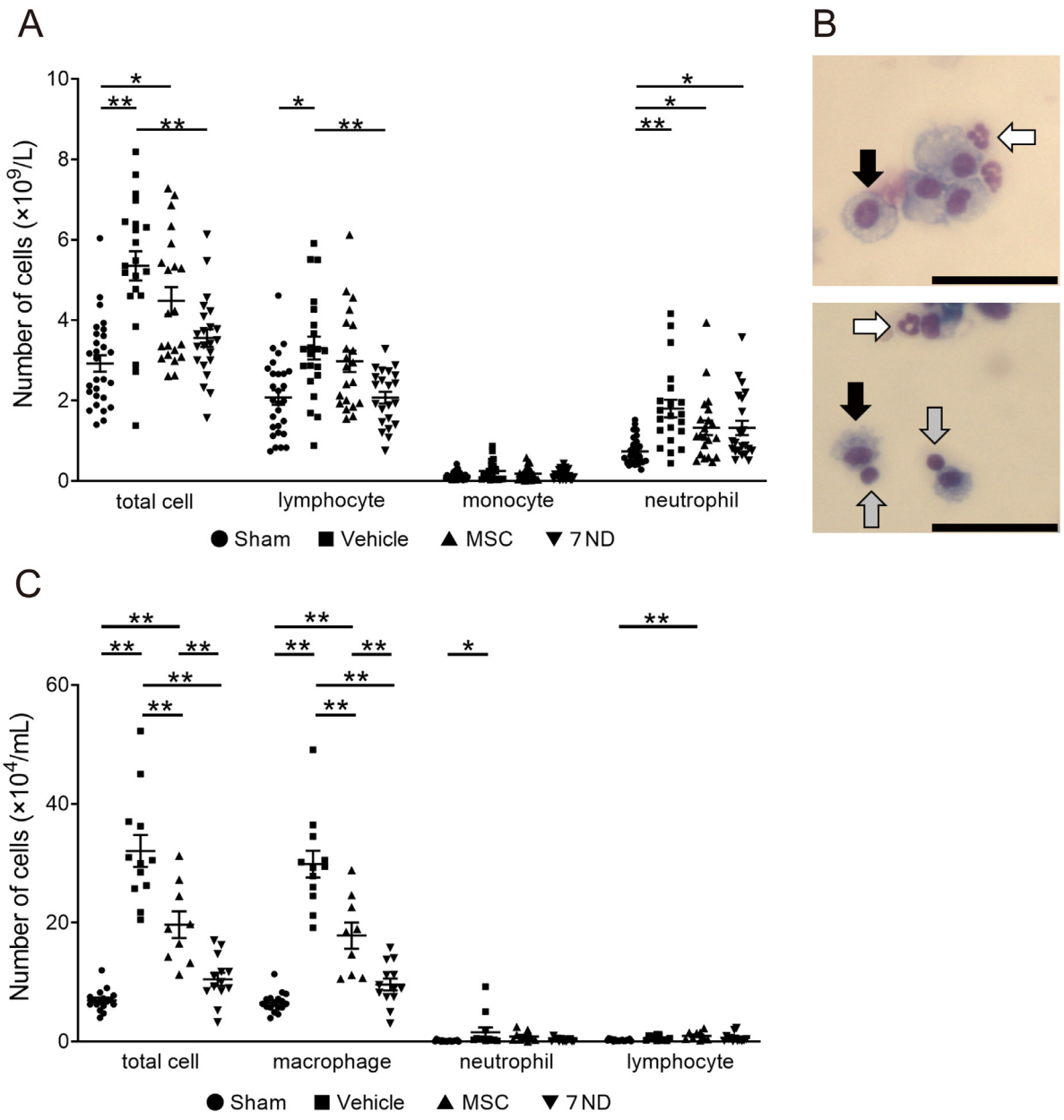

Figure 4. Impact of 7ND-MSCs on differential cell counts of blood and BALF. (A) Differential cell counts of blood at P15. The total cell and lymphocyte counts in the 7ND-treated groups were decreased compared with those in the vehicle- and control MSC-treated groups. The monocyte and neutrophil counts were not statistically different among the three groups exposed to hyperoxia. n = 29 for sham, 21 for vehicle, 20 for MSC and 22 for 7ND. $^{*}P < 0.05$ and $^{**}P < 0.01$. (B) Representative image of BALF cells with May–Giemsa staining. Black, white and gray arrows indicate macrophages, neutrophils and lymphocytes, respectively. Scale bars indicate 50 μm. (C) Differential cell counts of BALF at P15. The total cell and macrophage counts were significantly decreased in the 7ND-MSC–treated group compared with those in the vehicle- and control MSC-treated groups. The neutrophil and lymphocyte counts were not statistically different among the three groups exposed to hyperoxia. n = 17 for sham, 12 for vehicle, 9 for MSC and 13 for 7ND. $^{*}P < 0.05$ and $^{**}P < 0.01$.

the three groups exposed to hyperoxia (Supplementary Figure 1). Concerning S_A, hyperoxia in the vehicle, control MSC-treated and 7ND-MSC–treated groups induced a significantly lower S_A. However, the S_A in the 7ND-MSC–treated group was significantly improved compared with that in the vehicle group ($P < 0.01$). In contrast, no significant difference was found between the vehicle- and control MSC-treated groups (Figure 3D)

Impact of 7ND-MSCs on differential cell counts of blood and BALF

Accumulation of inflammatory cells in the blood and BALF was examined to evaluate systemic and airway inflammation. The total white blood cell and differential cell counts were measured using a fully automated differential hematology analyzer. Hyperoxia (vehicle group) increased the number of inflammatory cells, and 7ND treatment, but not MSC treatment, decreased/suppressed the accumulation of the inflammatory cells, particularly lymphocytes, compared with those in the vehicle group ($P < 0.01$, 7ND vs. vehicle; $P = 0.0886$, 7ND vs. MSC; n = 29 for sham, 21 for vehicle, 20 for MSC and 22 for 7ND; Figure 4A). No statistical difference was found in the number of monocytes and neutrophils among the three treatment groups.

The total cell number in BALF was counted using Burker chambers, and differential cell counts were evaluated using centrifuged preparations stained with May-Giemsa staining (Figure 4B). The numbers of total cells and macrophages in BALF were significantly increased in the vehicle group, and those in the 7ND-MSC–treated

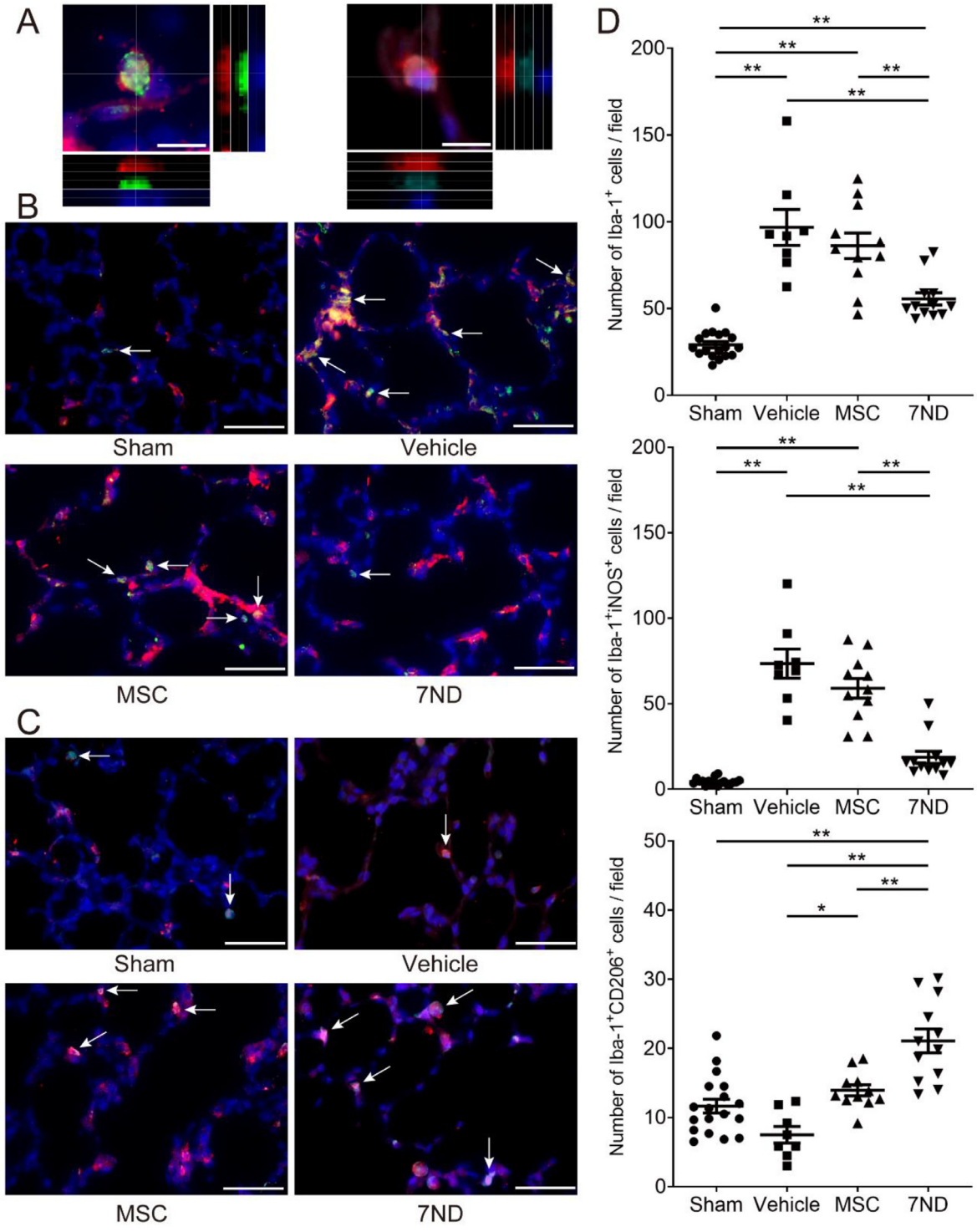

Figure 5. Macrophage polarization after 7ND-MSC and control MSC administration. (A) Representative pictures of Iba-1/iNOS (left) or CD206 (right) double-positive cells. Z-stacks were created to verify that they were truly double-positive. Scale bars indicate 10 μm. (B, C) Representative pictures of immunofluorescence staining for Iba-1 (red), iNOS (green) and DAPI (blue) (B) and Iba-1 (red), CD206 (light blue) and DAPI (blue) (C). Iba-1/iNOS or CD206 double-positive cells are indicated by white arrows. Scale bars indicate 50 μm. (D) Number of Iba-1–positive cells, Iba-1/iNOS double-positive cells and Iba-1/CD206 double-positive cells. The number of Iba-1/iNOS double-positive cells was significantly lower and that of Iba-1/CD206 double-positive cells was significantly higher in the 7ND-MSC–treated group compared with the vehicle- and control MSC-treated groups. n = 18 for sham, 8 for vehicle, 11 for MSC and 12 for 7ND. $^{*}P < 0.05$ and $^{**}P < 0.01$.

group were lower than those in the vehicle- and control MSC-treated groups ($P < 0.01$, n = 17 for sham, 12 for vehicle, 9 for MSC and 13 for 7ND; Figure 4C). No statistical difference was found in the numbers of neutrophils and lymphocytes among the three treatment groups (Figure 4C).

M1/M2 polarization of macrophages after administration of 7ND-MSCs and control MSCs

To discriminate the macrophage polarity in the lungs, we performed immunofluorescence staining with lung tissue sections for

Iba-1 (pan-macrophage marker), iNOS (M1 macrophage marker) and CD206 (M2 macrophage marker). We counted Iba-1/iNOS double-positive cells as M1 macrophages and Iba-1/CD206 double-positive cells as M2 macrophages. Representative photomicrographs are shown in Figure 5A, 5B and 5C. The total numbers of Iba-1–positive cells and Iba-1/iNOS double-positive cells were increased in the vehicle group but significantly decreased in the 7ND-MSC–treated group compared with the vehicle- and MSC-treated groups ($P < 0.01$; Figure 5D). In contrast, the number of Iba-1/CD206 double-positive cells was significantly increased in the 7ND-MSC–treated group compared with the vehicle- and MSC-treated groups ($P < 0.01$, 7ND vs. vehicle; $P < 0.05$, 7ND vs. MSC; n = 18 for sham, 8 for vehicle, 11 for MSC and 12 for 7ND; Figure 5D), indicating that intravenous injection of 7ND-MSCs, but not MSCs, decreased and/or suppressed the increased number of macrophages in the lung and changed the polarity of M1 macrophages into M2 macrophages.

Impact of 7ND-MSCs on pulmonary artery remodeling

To determine the effects of 7ND-MSC on pulmonary vascular remodeling, immunofluorescence staining for α-SMA was performed with lung paraffin sections, and MWT was assessed. In the BPD model (vehicle group), the peripheral pulmonary arteries showed increased α-SMA expression, and the MWT was significantly higher compared with the sham rats. However, 7ND-MSC treatment decreased α-SMA expression, and MWT was significantly lower compared with the vehicle- and MSC-treated groups ($P < 0.01$, 7ND vs. vehicle; $P < 0.05$, 7ND vs. MSC; n = 3 for sham, 3 for vehicle, 5 for MSC and 4 for 7ND; Figure 6A and 6B). Furthermore, to evaluate vascular smooth cell proliferation by pulmonary vascular remodeling, double immunofluorescence staining for α-SMA and Ki-67 was performed, and the percentage of vessels stained positively for Ki-67 was assessed. A representative photomicrograph of a Ki-67/α-SMA double-positive cell is shown in Figure 6C. The percentage of Ki-67–positive vessels was significantly increased in the vehicle group compared with that in the sham group, and lower in the 7ND-MSC–treated group ($P < 0.01$), but not in the MSC group (n = 18 for sham, 8 for vehicle, 11 for MSC and 12 for 7ND; Figure 6D). These results suggested that 7ND-MSCs, but not MSCs, ameliorated the pulmonary arteriolar muscularization and smooth muscle cell proliferation by vascular remodeling.

Impact of 7ND-MSCs on PH

RV/LV+S and RVSP were assessed to evaluate the effects of 7ND-MSCs on PH. BPD induced PH, which was significantly indicated by both RV/LV+S and RVSP. Compared with the vehicle- and MSC-treated groups, the 7ND-MSC–treated group had a significant decrease in RV/LV+S ($P < 0.01$; n = 24 for sham, 12 for vehicle, 17 for MSC and 17 for 7ND; Figure 7A), suggesting improvement of right ventricular hypertrophy. Moreover, the RVSP of the 7ND-MSC–treated group was significantly reduced compared with the vehicle- and MSC-treated groups ($P < 0.01$, 7ND vs. vehicle; $P < 0.05$, 7ND vs. MSC; n = 5 for sham, 6 for vehicle, 6 for MSC and 6 for 7ND; Figure 7B).

Impact of 7ND-MSCs on messenger RNA expressions in the lung tissue

The messenger RNA (mRNA) expression of IL-6 and CCL2 was analyzed using quantitative RT-PCR to evaluate the molecular biological effect of 7ND-MSCs in the lung tissue. Quantitative RT-PCR showed that BPD (hyperoxia; vehicle group) increased IL-6 and CCL2 expressions in the lungs, whereas 7ND-MSCs decreased their mRNA expressions. MSCs tended to decrease their expression, but not significantly (n = 19 for sham, 10 for vehicle, 15 for MSC and 15 for 7ND; Figure 8). 7ND-MSCs had a significantly higher ability to decrease CCL2 production than MSCs.

Discussion

In the present study, we demonstrated that intravenous administration of 7ND-MSCs had a therapeutic effect on hyperoxia-induced inhibition of alveolarization in rats by decreasing/suppressing inflammation. In addition, BPD-associated PH was also ameliorated by 7ND-MSCs.

The pathology of BPD is a lung injury pattern characterized by impaired alveolarization, including inflammation, bronchial smooth muscle thickening and interstitial edema [41,42]. The hyperoxia-induced lung injury in neonatal rats is similar to this pattern, resulting in fewer and larger alveoli and thickened alveolar septa in the lung [31,43]. In the present study, expansion of the alveolar space was observed in the BPD model rats (vehicle-treated group), and their VD_T and S_A were decreased.

The most important finding of our present study is the significant improvement of VD_T and S_A after 7ND-MSC administration compared with the vehicle, but almost no improvement was found with control MSCs, indicating that 7ND-MSCs ameliorated impaired alveolarization more than the control MSCs. The therapeutic effect of 7ND-MSCs is further enhanced by the effect of 7ND compared with MSCs alone. One of the possible mechanisms underlying this positive effect was the reduction/suppression of alveolar inflammation by 7ND-MSC administration. 7ND-MSCs secrete 7ND, a deletion mutant of human CCL2, which inhibits CCL2 that regulate migration and infiltration of monocytes/macrophages [23]. Therefore, we expected that 7ND-MSCs have a particularly powerful effect of suppressing macrophages compared with MSCs. In the present study, 7ND-MSC administration at P5 significantly decreased the accumulation of inflammatory cells, particularly macrophages, in BALF. Moreover, M1 macrophages were mainly reduced and M2 macrophages were increased in the 7ND-MSC–treated group compared with the treatment of MSCs alone. Macrophages are divided into two types as follows: the pro-inflammatory (M1) and anti-inflammatory (M2) types. M1 macrophages play a critical role in the initiation of acute lung injury [44,45]. This result suggested that the inflammatory reaction by alveolar macrophages (M1) in the lung tissue may be suppressed by 7ND-MSC administration and 7ND-MSCs may promote the change of macrophage polarization from M1 to M2.

Recently, there are a growing number of reports that highlight the complexity of lung myeloid compartments, including alveolar macrophages as well as various subsets of non-alveolar macrophages, such as dendritic cells, tissue monocytes and interstitial macrophages [46]. In the present study, we did not evaluate in detail, but we performed immunostaining of Iba-1, CD11b and c-mer proto-oncogene tyrosine kinase (MerTK) as a preliminary experiment. The staining seemed that the hyperoxia exposure (vehicle group) increased the number of Iba-1–positive/CD11b and MerTK-negative cells and Iba-1/CD11b double-positive/MerTK-negative cells compared with the sham group, and 7ND-MSC treatment suppressed the elevations. In contrast, Iba-1/CD11b/MerTK triple-positive cells seemed to be almost unchanged (Supplementary Figure 2). According to previous reports [46], these Iba-1–positive cells may contain some interstitial macrophages as Iba-1/CD11b/MerTK triple-positive cells and/or some classical dendritic cells as Iba-1–positive/CD11b and MerTK-negative cells or Iba-I/CD11b double-positive/MerTK-negative cells. Because it is controversial whether or not Iba-1–positive cells contain alveolar macrophages [47–49], it was difficult to show what kinds of cells constitute the Iba-1–positive cells in the present study. We will evaluate this in detail in the subsequent studies.

In addition, 7ND-MSCs may also have some effect on immune cells other than macrophages. In our experiment, the number of total inflammatory cells in the blood, particularly lymphocytes, in the 7ND-MSC–treated group was lower than that in the vehicle- and control MSC-treated groups, showing that 7ND-MSC administration improved nonspecific inflammation systemically as well as in the

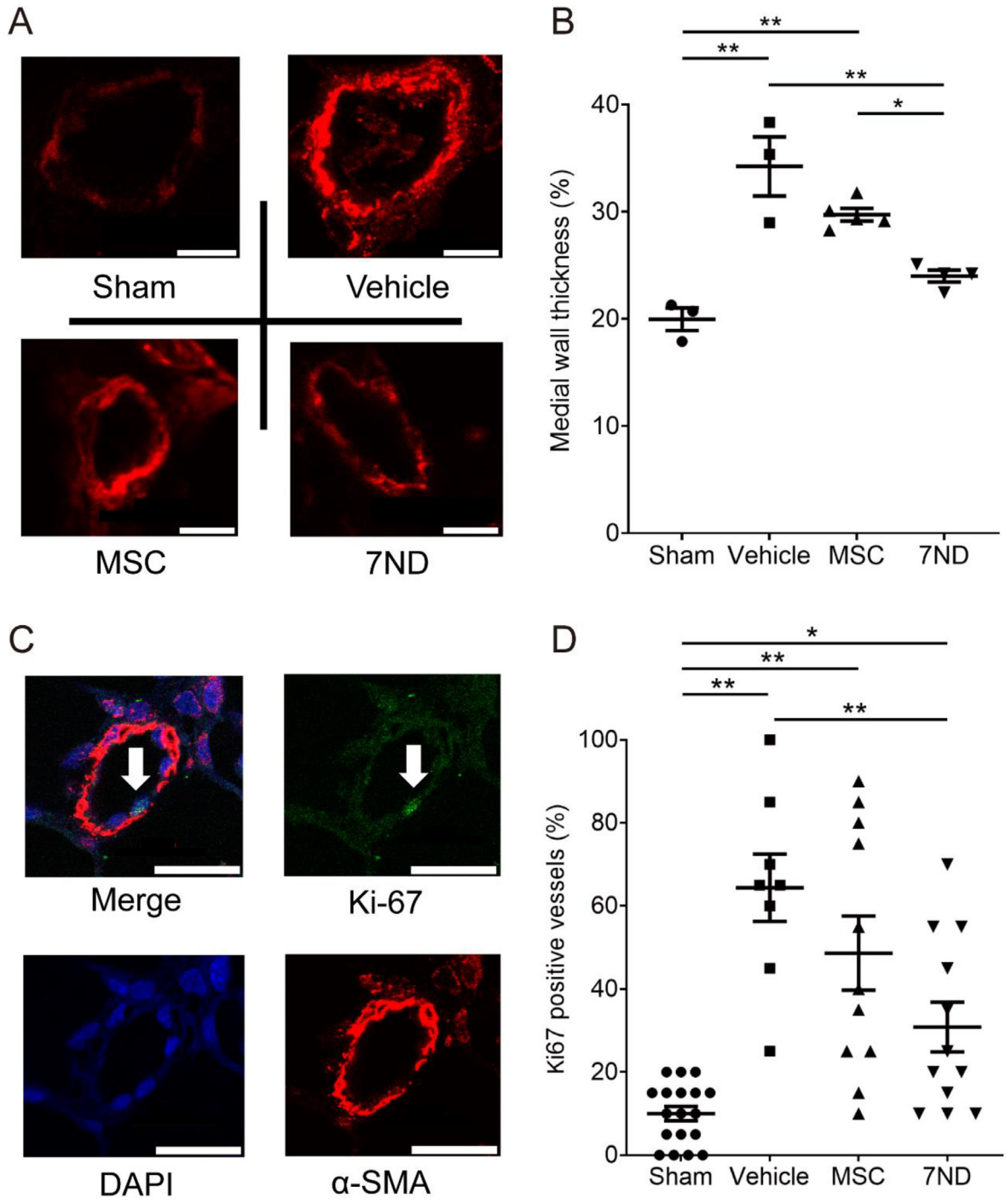

Figure 6. Impact of 7ND-MSCs on pulmonary artery remodeling. (A) Immunofluorescence staining for α-SMA. Scale bars indicate 10 μm. (B) MWT at P15. The MWT in the 7ND-MSC–treated group was significantly lower than that in the vehicle- and control MSC-treated groups. n = 3 for sham, 3 for vehicle, 5 for MSC and 4 for 7ND. $^{*}P < 0.05$ and $^{**}P < 0.01$. (C) Representative pictures of immunofluorescence staining for α-SMA (red), Ki-67 (green) and DAPI (blue). White arrows indicate Ki-67–positive cells. Scale bars indicate 20 μm. (D) Percentage of Ki-67–positive vessels at P15 in each experimental group. The percentage of Ki-67–positive vessels in the 7ND-MSC–treated group was significantly lower than that in the vehicle-treated group. The percentage of Ki-67–positive cells tended to decrease in the 7ND-MSC–treated group compared with that in the control MSC-treated group, but was not statistically significant. n = 18 for sham, 8 for vehicle, 11 for MSC and 12 for 7ND. $^{*}P < 0.05$ and $^{**}P < 0.01$.

lung. In *ex vivo* imaging, both 7ND-MSC and control MSC were distributed mainly in the lungs and liver within 3 h and then remained until 7 days after injection. Even in the spleen and kidney, to a small extent, both cells were distributed up to 7 days after the injection (Supplementary Figure 3). These results reinforce the possibility that 7ND-MSC has systemic anti-inflammatory effects through distribution to various organs after intravenous injection.

In the present study, the therapeutic effect of 7ND-MSC in PH was also demonstrated compared with control MSC. PH in BPD significantly impacts the morbidity and mortality in neonates [50,51]. The pathobiology of PH in BPD is characterized by inflammation and dysmorphic angiogenesis, resulting in fewer (small) pulmonary arteries and frequently in pulmonary hypertensive vascular disease [52–54]. Pulmonary hypertensive vascular disease in hyperoxia-induced BPD

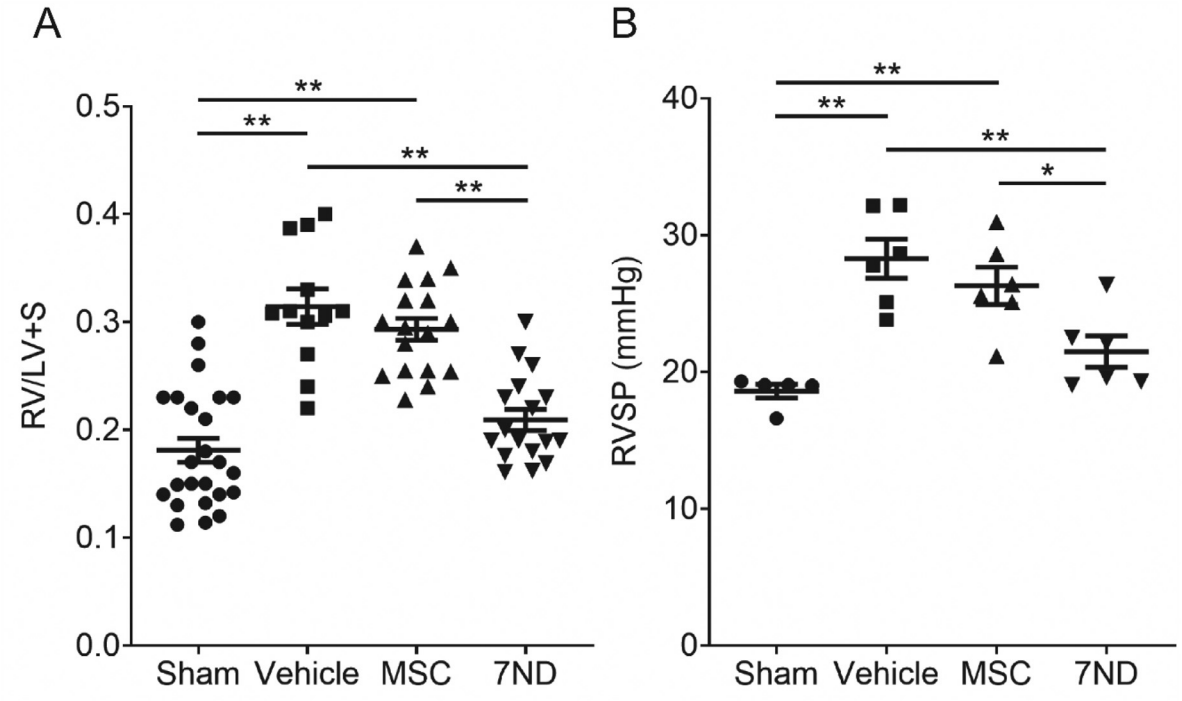

Figure 7. Impact of 7ND-MSCs on pulmonary hypertension. (A) RV/LV+S at P15. RV/LV+S, as an indicator of right ventricular hypertrophy, in the 7ND-MSC–treated group was significantly lower than that in the vehicle- and control MSC-treated groups. n = 24 for sham, 12 for vehicle, 17 for MSC and 17 for 7ND. $^{*}P < 0.05$ and $^{**}P < 0.01$. (B) RVSP at P15. The RVSP in the 7ND-MSC–treated group was significantly decreased compared with that in the vehicle- and control MSC-treated groups. n = 5 for sham, 6 for vehicle, 6 for MSC and 6 for 7ND. $^{*}P < 0.05$ and $^{**}P < 0.01$.

causes pulmonary arteriolar muscularization, profound remodeling of peripheral pulmonary vessels and right ventricular hypertrophy [55–57]. Because smooth muscle cell proliferation and vascular remodeling increase pulmonary arterial resistance and elevate right ventricular systolic blood pressure, improving these conditions is important in the development and progression of PH [42,53,58,59].

In the present study, 7ND-MSCs ameliorated right ventricular hypertrophy, which was shown by the improved dry weight ratio

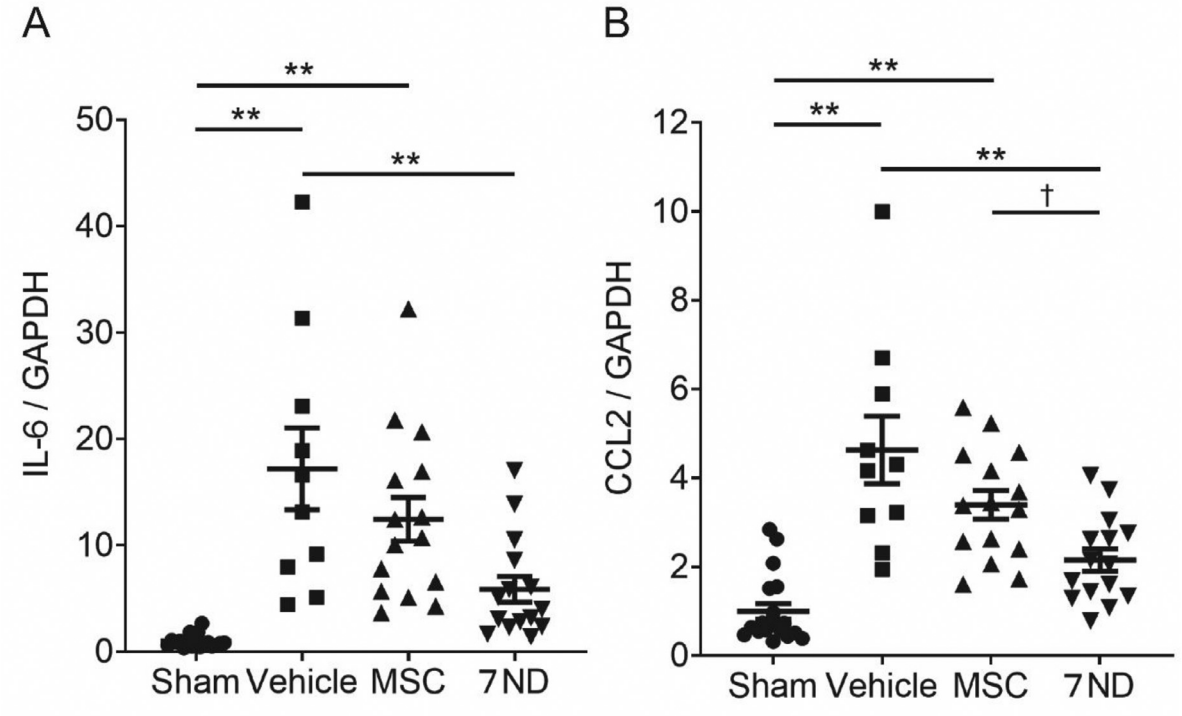

Figure 8. Impact of 7ND-MSCs on mRNA expressions in lung tissue. The mRNA expressions of IL-6 and CCL2 were significantly decreased in the 7ND-MSC–treated group compared with the vehicle-treated group. Compared with the control MSC-treated group, the 7ND-MSC–treated group tended to have lower mRNA expressions of IL-6 and CCL2, but was not statistically significant. n = 19 for sham, 10 for vehicle, 15 for MSC and 15 for 7ND. $^{\dagger}P = 0.0841$ and $^{**}P < 0.01$.

(RV/LV+S), and reduced percentage of muscularized pulmonary arteries. In addition, our results also showed that 7ND-MSCs suppressed smooth muscle cell proliferation and vascular remodeling. Thus, the right ventricular systolic blood pressure in the 7ND-MSC–treated group was significantly decreased, indicating that 7ND-MSCs have a therapeutic effect on PH in hyperoxia-induced BPD.

Aslam *et al.* showed that MSCs reduced lung vascular injury and prevented PH in a BPD model [60]. Interestingly, in the present study, the therapeutic effect of 7ND-MSCs on PH, which combined the effect of 7ND and MSCs, was even higher than that of MSCs alone. Several studies showed that 7ND is effective for PH [61,62]. Ikeda *et al.* showed that intramuscular gene transfer of 7ND monocyte chemoattractant protein-1 (MCP-1) cDNA suppressed disease progression of monocrotaline-induced PH by suppressing monocyte/macrophage recruitment and the systemic MCP-1 signaling pathway. It is unknown whether the prominent therapeutic effect of 7ND-MSCs on PH is a macrophage inhibitory effect by 7ND or a cell therapy effect by MSC. Whatever is the prominent factor for the treatment, the present study, indicating that 7ND-MSCs improved PH more effectively than MSCs alone, showed that using 7ND-MSCs is significant for PH treatment.

The impact of 7ND-MSC administration on the mRNA expression of inflammatory cytokines/chemokines in the lung tissue was evaluated to further elucidate the mechanisms of 7ND-MSC therapy and support the finding of reduced inflammation. Thompson and Bhandari have found higher levels of proinflammatory cytokines (IL-1b, IL-6 and IL-16) and lower levels of anti-inflammatory cytokines (IL-10 and IL-13) in premature infants with BPD [63]. In some studies, these elevations were improved even by MSC administration alone [36,64]. Interestingly, we showed that the mRNA expressions of IL-6 and CCL2 in the lung in the 7ND-MSC–treated group were further suppressed compared with treatment MSC alone. Because 7ND has a suppressive effect on CCL2, which activates alveolar macrophage-induced lung injury [65], CCL2 suppression by 7ND-MSCs may reduce inflammatory cytokines such as IL-6. This result complements that the effect of 7ND-MSC to reduce inflammation is further enhanced by the effect of 7ND suppressing CCL2 compared with MSC alone.

The present study has several limitations. First, although 7ND-MSCs have shown therapeutic effects of improving lung tissue injury and PH, the survival rate was not significantly different. However, 7ND-MSCs also showed a significant increase in body weight compared with vehicle on P15. Sutsko *et al.* reported that MSC administration provided long-term repair of the neonatal hyperoxia-injured lung [66]. 7ND-MSCs are also expected to have a long-term therapeutic effect. Lung tissue injury and PH induced by BPD last for a long period after hyperoxia [50]. Thus, performing longer-term assessment to confirm survival rate might be better. Moreover, there are various cell doses in studies using MSCs for BPD [15,60,67,68]. We intravenously administered MSCs and 7ND-MSCs at 1×10^5 cells/pup, considering the body weight of neonatal rats. The treatment effect of the stem cells was known to be dose-dependent [69]. By contrast, a large amount of MSCs has been shown to cause side effects, such as pulmonary embolism [70]. Considering the clinical application, the higher the number of cells we could administer, the higher the risk and cost the patient could have. In addition, to perform safe and certain intravenous injection to small pups, we decided to set the timing of cells administered to P5 based on the results in previous reports [15]. There is a report that early cell administration is more effective for BPD [71]. Thus, our 7ND-MSC dose might not be appropriate. Further analysis is required to investigate the appropriate dose and timing of 7ND-MSC administration.

Second, we compared the therapeutic effect only between MSCs and 7ND-MSCs, but not 7ND alone. When 7ND is administrated systemically (intravenously), accumulation of 7ND is expected to be little. By contrast, intratracheal administration of 7ND may be more effective in the lung, but it may lead to a weakened effect of suppressing systemic inflammation. MSCs are expected to be used not only as stem cells but also as vehicles for gene expression because MSCs accumulate at the site of lung injury [72]. Therefore, it is conceivable that 7ND-MSCs accumulate in the lung more efficiently and suppress systemic inflammation more effectively compared with 7ND alone. Moreover, 7ND-MSCs can also exert trophic effects, such as anti-inflammatory, tissue protective and immunosuppressive effects, similar to MSCs. It is unknown whether MSCs alone or 7ND alone is more effective for BPD. However, for these reasons, 7ND-MSCs should be more effective than 7ND alone.

Finally, the safety of 7ND-MSCs has not been confirmed. Because 7ND-MSCs use lentiviral introduction, it is undeniable that some side effects might possibly develop. However, in the present study, 7ND-MSC administration did not decrease the survival rate or show tumorigenesis in each organ, although long-term evaluation was not performed. Moreover, no clinical trial used 7ND-MSCs, but clinical trials that used MSCs alone for BPD have been ongoing [73,74]. Several basic studies and clinical trials on various diseases have been conducted for 7ND [75–77]. Because the safety of both 7ND and MSCs has been confirmed independently, adverse events are less likely to occur even if 7ND and MSCs are combined. Taken together, considering clinical application, intravenous administration of 7ND-MSC is a viable treatment.

In conclusion, we have demonstrated that intravenous administration of 7ND-MSCs improved hyperoxia-induced lung pathology and PH in neonatal rats compared with MSCs. Improvements in alveolar maldevelopment and vasculature remodeling are shown to be associated with downregulation of 7ND targets, including CCL2 and IL-6, regulating inflammation and suppression of alveolar macrophages, particularly M1 macrophages. Thus, the effects of 7ND-MSCs in neonatal BPD lungs are likely mediated by paracrine mechanisms of both MSCs and 7ND. Therefore, intravenous administration of 7ND-MSCs may be a novel strategy in the treatment of BPD.

Declaration of Competing Interest

The authors have no commercial, proprietary, or financial interest in the products or companies described in this article.

Funding

This work was supported by the Japan Society for the Promotion of Science (JSPS) KAKENHI (grant numbers 16K15534 and 18K15667).

Author Contributions

Conception and design of the study: TS, YoS, TK, YT, TN, and MH. Cell preparation: SS, and TN. Acquisition of data: TS, HY, HM, YuS and AO. Analysis and interpretation of data: TS, YoS, YK, KU, and TN. Drafting or revising the manuscript: TS, YoS, TK, KU, YT, TN, and MH. All authors have approved the final article.

Acknowledgements

We are grateful to Dr. Kenji Wakabayashi for helpful discussion and Ms. Kimi Watanabe, Ms. Eiko Aoki, Ms. Tokiko Nishino, Ms. Azusa Okamoto and Ms. Tomoko Yamaguchi for the skillful technical assistance.

Supplementary materials

Supplementary material associated with this article can be found in the online version at doi:10.1016/j.jcyt.2020.01.009.

References

[1] Kalikkot Thekkeveedu R, Guaman MC, Shivanna B. Bronchopulmonary dysplasia: A review of pathogenesis and pathophysiology. Respir Med 2017;132:170–7.
[2] Jobe AH, Bancalari E. Bronchopulmonary dysplasia. Am J Respir Crit Care Med 2001;163(7):1723–9.
[3] Davidson LM, Berkelhamer SK. Bronchopulmonary Dysplasia: Chronic Lung Disease of Infancy and Long-Term Pulmonary Outcomes. J Clin Med 2017;6(1):4.
[4] Pakvasa MA, Saroha V, Patel RM. Optimizing Caffeine Use and Risk of Bronchopulmonary Dysplasia in Preterm Infants: A Systematic Review, Meta-analysis, and Application of Grading of Recommendations Assessment, Development, and Evaluation Methodology. Clin Perinatol 2018;45(2):273–91.
[5] Dumpa V, Bhandari V. Surfactant, steroids and non-invasive ventilation in the prevention of BPD. Semin Perinatol 2018;42(7):444–52.
[6] Iyengar A, Davis JM. Drug therapy for the prevention and treatment of bronchopulmonary dysplasia. Front Pharmacol 2015;6:12.
[7] van Velthoven CT, Sheldon RA, Kavelaars A, Derugin N, Vexler ZS, Willemen HL, Maas M, Heijnen CJ, Ferriero DM. Mesenchymal stem cell transplantation attenuates brain injury after neonatal stroke. Stroke 2013;44(5):1426–32.
[8] de Witte SFH, Merino AM, Franquesa M, Strini T, van Zoggel JAA, Korevaar SS, Luk F, Gargesha M, O'Flynn L, Roy D, Elliman SJ, Newsome PN, Baan CC, Hoogduijn MJ. Cytokine treatment optimises the immunotherapeutic effects of umbilical cord-derived MSC for treatment of inflammatory liver disease. Stem Cell Res Ther 2017;8(1):140.
[9] Liu Y, Hu J, Wang S. Mesenchymal stem cell-mediated treatment of oral diseases. Histol Histopathol 2014;29(8):1007–15.
[10] Sugiyama Y, Sato Y, Kitase Y, Suzuki T, Kondo T, Mikrogeorgiou A, Horinouchi A, Maruyama S, Shimoyama Y, Tsuji M, Suzuki S, Yamamoto T, Hayakawa M. Intravenous Administration of Bone Marrow-Derived Mesenchymal Stem Cell, but not Adipose Tissue-Derived Stem Cell, Ameliorated the Neonatal Hypoxic-Ischemic Brain Injury by Changing Cerebral Inflammatory State in Rat. Front Neurol 2018;9(757):757.
[11] Porzionato A, Zaramella P, Dedja A, Guidolin D, Van Wemmel K, Macchi V, Jurga M, Perilongo G, De Caro R, Baraldi E, Muraca M. Intratracheal administration of clinical-grade mesenchymal stem cell-derived extracellular vesicles reduces lung injury in a rat model of bronchopulmonary dysplasia. Am J Physiol Lung Cell Mol Physiol 2019;316(1):L6–L19.
[12] Braun RK, Chetty C, Balasubramaniam V, Centanni R, Haraldsdottir K, Hematti P, Eldridge MW. Intraperitoneal injection of MSC-derived exosomes prevent experimental bronchopulmonary dysplasia. Biochem Biophys Res Commun 2018;503(4):2653–8.
[13] Tropea KA, Leder E, Aslam M, Lau AN, Raiser DM, Lee JH, Balasubramaniam V, Fredenburgh LE, Alex Mitsialis S, Kourembanas S, Kim CF. Bronchioalveolar stem cells increase after mesenchymal stromal cell treatment in a mouse model of bronchopulmonary dysplasia. Am J Physiol Lung Cell Mol Physiol 2012;302(9):L829–37.
[14] Pierro M, Ciarmoli E, Thebaud B. Bronchopulmonary Dysplasia and Chronic Lung Disease: Stem Cell Therapy. Clin Perinatol 2015;42(4):889–910.
[15] Augustine S, Avey MT, Harrison B, Locke T, Ghannad M, Moher D, Thebaud B. Mesenchymal Stromal Cell Therapy in Bronchopulmonary Dysplasia: Systematic Review and Meta-Analysis of Preclinical Studies. Stem Cells Transl Med 2017;6(12):2079–93.
[16] Shahzad T, Radajewski S, Chao C-M, Bellusci S, Ehrhardt H. Pathogenesis of bronchopulmonary dysplasia: when inflammation meets organ development. Molecular and Cellular Pediatrics 2016;3(1):23.
[17] Duffy MM, Ritter T, Ceredig R, Griffin MD. Mesenchymal stem cell effects on T-cell effector pathways. Stem Cell Res Ther 2011;2(4):34.
[18] Zeng SL, Wang LH, Li P, Wang W, Yang J. Mesenchymal stem cells abrogate experimental asthma by altering dendritic cell function. Mol Med Rep 2015;12(2):2511–20.
[19] Milosavljevic N, Gazdic M, Simovic Markovic B, Arsenijevic A, Nurkovic J, Dolicanin Z, Djonov V, Lukic ML, Volarevic V. Mesenchymal stem cells attenuate acute liver injury by altering ratio between interleukin 17 producing and regulatory natural killer T cells. Liver Transpl 2017;23(8):1040–50.
[20] Carty F, Mahon BP, English K. The influence of macrophages on mesenchymal stromal cell therapy: passive or aggressive agents? Clin Exp Immunol 2017;188(1):1–11.
[21] Zhang YJ, Rollins BJ. A Dominant-Negative Inhibitor Indicates That Monocyte Chemoattractant Protein-1 Functions as a Dimer. Mol Cell Biol 1995;15(9):4851–5.
[22] Shimizu H, Maruyama S, Yuzawa Y, Kato T, Miki Y, Suzuki S, Sato W, Morita Y, Maruyama H, Egashira K, Matsuo S. Anti-monocyte chemoattractant protein-1 gene therapy attenuates renal injury induced by protein-overload proteinuria. J Am Soc Nephrol 2003;14(6):1496–505.
[23] Deshmane SL, Kremlev S, Amini S, Sawaya BE. Monocyte chemoattractant protein-1 (MCP-1): an overview. J Interferon Cytokine Res 2009;29(6):313–26.
[24] Zaloudikova M, Vytasek R, Vajnerova O, Hnilickova O, Vizek M, Hampl V, Herget J. Depletion of Alveolar Macrophages Attenuates Hypoxic Pulmonary Hypertension but not Hypoxia-Induced Increase in Serum Concentration of MCP-1. Physiol Res 2016;65(5):763–8.
[25] Kimura H, Okada O, Tanabe N, Tanaka Y, Terai M, Takiguchi Y, Masuda M, Nakajima N, Hiroshima K, Inadera H, Matsushima K, Kuriyama T. Plasma monocyte chemoattractant protein-1 and pulmonary vascular resistance in chronic thromboembolic pulmonary hypertension. Am J Resp Crit Care 2001;164(2):319–24.
[26] Steiner MK, Syrkina OL, Kolliputi N, Mark EJ, Hales CA, Waxman AB. Interleukin-6 overexpression induces pulmonary hypertension. Circ Res 2009;104(2):236–44. 28p following 244.
[27] Saka Y, Furuhashi K, Katsuno T, Kim H, Ozaki T, Iwasaki K, Haneda M, Sato W, Tsuboi N, Ito Y, Matsuo S, Kobayashi T, Maruyama S. Adipose-derived stromal cells cultured in a low-serum medium, but not bone marrow-derived stromal cells, impede xenoantibody production. Xenotransplantation 2011;18(3):196–208.
[28] Saito S, Nakayama T, Hashimoto N, Miyata Y, Egashira K, Nakao N, Nishiwaki S, Hasegawa M, Hasegawa Y, Naoe T. Mesenchymal stem cells stably transduced with a dominant-negative inhibitor of CCL2 greatly attenuate bleomycin-induced lung damage. Am J Pathol 2011;179(3):1088–94.
[29] Snyder JM, Jenkins-Moore M, Jackson SK, Goss KL, Dai HH, Bangsund PJ, Giguere V, McGowan SE. Alveolarization in retinoic acid receptor-beta-deficient mice. Pediatr Res 2005;57(3):384–91.
[30] Hsia CC, Hyde DM, Ochs M, Weibel ER. An official research policy statement of the American Thoracic Society/European Respiratory Society: standards for quantitative assessment of lung structure. Am J Respir Crit Care Med 2010;181(4):394–418.
[31] Choi CW, Kim BI, Hong JS, Kim EK, Kim HS, Choi JH. Bronchopulmonary dysplasia in a rat model induced by intra-amniotic inflammation and postnatal hyperoxia: morphometric aspects. Pediatr Res 2009;65(3):323–7.
[32] Basu RK, Donaworth E, Wheeler DS, Devarajan P, Wong HR. Antecedent acute kidney injury worsens subsequent endotoxin-induced lung inflammation in a two-hit mouse model. Am J Physiol Renal Physiol 2011;301(3):F597–604.
[33] Zhang C, Lei GS, Shao S, Jung HW, Durant PJ, Lee CH. Accumulation of myeloid-derived suppressor cells in the lungs during Pneumocystis pneumonia. Infect Immun 2012;80(10):3634–41.
[34] Ito T, Okada T, Miyashita H, Nomoto T, Nonaka-Sarukawa M, Uchibori R, Maeda Y, Urabe M, Mizukami H, Kume A, Takahashi M, Ikeda U, Shimada K, Ozawa K. Interleukin-10 expression mediated by an adeno-associated virus vector prevents monocrotaline-induced pulmonary arterial hypertension in rats. Circ Res 2007;101(7):734–41.
[35] Wagenaar GT, Laghmani el H, Fidder M, Sengers RM, de Visser YP, de Vries L, Rink R, Roks AJ, Folkerts G, Walther FJ. Agonists of MAS oncogene and angiotensin II type 2 receptors attenuate cardiopulmonary disease in rats with neonatal hyperoxia-induced lung injury. Am J Physiol Lung Cell Mol Physiol 2013;305(5):L341–51.
[36] Rong M, Chen S, Zambrano R, Duncan MR, Grotendorst G, Wu S. Inhibition of beta-catenin signaling protects against CTGF-induced alveolar and vascular pathology in neonatal mouse lung. Pediatr Res 2016;80(1):136–44.
[37] Young KC, Torres E, Hehre D, Wu S, Suguihara C, Hare JM. Antagonism of stem cell factor/c-kit signaling attenuates neonatal chronic hypoxia-induced pulmonary vascular remodeling. Pediatr Res 2016;79(4):637–46.
[38] Pansani MC, Azevedo PS, Rafacho BP, Minicucci MF, Chiuso-Minicucci F, Zorzella-Pezavento SG, Marchini JS, Padovan GJ, Fernandes AA, Matsubara BB, Matsubara LS, Zornoff LA, Paiva SA. Atrophic cardiac remodeling induced by taurine deficiency in Wistar rats. PLoS One 2012;7(7):e41439.
[39] Kishimoto Y, Kato T, Ito M, Azuma Y, Fukasawa Y, Ohno K, Kojima S. Hydrogen ameliorates pulmonary hypertension in rats by anti-inflammatory and antioxidant effects. J Thorac Cardiovasc Surg 2015;150(3):645–54. e3.
[40] Meghwani H, Prabhakar P, Mohammed SA, Seth S, Hote MP, Banerjee SK, Arava S, Ray R, Maulik SK. Beneficial effects of aqueous extract of stem bark of Terminalia arjuna (Roxb.), An ayurvedic drug in experimental pulmonary hypertension. J Ethnopharmacol 2017;197:184–94.
[41] Husain AN, Siddiqui NH, Stocker JT. Pathology of arrested acinar development in postsurfactant bronchopulmonary dysplasia. Hum Pathol 1998;29(7):710–7.
[42] Coalson JJ. Pathology of new bronchopulmonary dysplasia. Semin Neonatol 2003;8(1):73–81.
[43] Randell SH, Mercer RR, Young SL. Neonatal hyperoxia alters the pulmonary alveolar and capillary structure of 40-day-old rats. Am J Pathol 1990;136(6):1259–66.
[44] Aggarwal NR, King LS, D'Alessio FR. Diverse macrophage populations mediate acute lung inflammation and resolution. Am J Physiol Lung Cell Mol Physiol 2014;306(8):L709–25.
[45] Lu HL, Huang XY, Luo YF, Tan WP, Chen PF, Guo YB. Activation of M1 macrophages plays a critical role in the initiation of acute lung injury. Biosci Rep 2018;38(2).
[46] Schyns J, Bureau F, Marichal T. Lung Interstitial Macrophages: Past, Present, and Future. J Immunol Res 2018(2018):5160794.
[47] Kohler C. Allograft inflammatory factor-1/Ionized calcium-binding adapter molecule 1 is specifically expressed by most subpopulations of macrophages and spermatids in testis. Cell Tissue Res 2007;330(2):291–302.
[48] Yamauchi K, Kasuya Y, Kuroda F, Tanaka K, Tsuyusaki J, Ishizaki S, Matsunaga H, Iwamura C, Nakayama T, Tatsumi K. Attenuation of lung inflammation and fibrosis in CD69-deficient mice after intratracheal bleomycin. Respir Res 2011;12:131.
[49] Donovan KM, Leidinger MR, McQuillen LP, Goeken JA, Hogan CM, Harwani SC, Flaherty HA, Meyerholz DK. Allograft Inflammatory Factor 1 as an Immunohistochemical Marker for Macrophages in Multiple Tissues and Laboratory Animal Species. Comp Med 2018;68(5):341–8.
[50] Berkelhamer SK, Mestan KK, Steinhorn RH. Pulmonary hypertension in bronchopulmonary dysplasia. Semin Perinatol 2013;37(2):124–31.
[51] Al-Ghanem G, Shah P, Thomas S, Banfield L, El Helou S, Fusch C, Mukerji A. Bronchopulmonary dysplasia and pulmonary hypertension: a meta-analysis. J Perinatol 2017;37(4):414–9.
[52] Altit G, Dancea A, Renaud C, Perreault T, Lands LC, Sant'Anna G. Pathophysiology, screening and diagnosis of pulmonary hypertension in infants with bronchopulmonary dysplasia - A review of the literature. Paediatr Respir Rev 2017;23:16–26.
[53] Bui CB, Pang MA, Sehgal A, Theda C, Lao JC, Berger PJ, Nold MF, Nold-Petry CA. Pulmonary hypertension associated with bronchopulmonary dysplasia in preterm infants. J Reprod Immunol 2017;124:21–9.
[54] Stocker JT. Pathologic features of long-standing "healed" bronchopulmonary dysplasia: a study of 28 3- to 40-month-old infants. Hum Pathol 1986;17(9):943–61.

[55] Hansmann G, Fernandez-Gonzalez A, Aslam M, Vitali SH, Martin T, Mitsialis SA, Kourembanas S. Mesenchymal stem cell-mediated reversal of bronchopulmonary dysplasia and associated pulmonary hypertension. Pulm Circ 2012;2(2):170–81.
[56] Heilman RP, Lagoski MB, Lee KJ, Taylor JM, Kim GA, Berkelhamer SK, Steinhorn RH, Farrow KN. Right ventricular cyclic nucleotide signaling is decreased in hyperoxia-induced pulmonary hypertension in neonatal mice. Am J Physiol Heart Circ Physiol 2015;308(12):H1575–82.
[57] de Visser YP, Walther FJ, Laghmani el H, Boersma H, van der Laarse A, Wagenaar GT. Sildenafil attenuates pulmonary inflammation and fibrin deposition, mortality and right ventricular hypertrophy in neonatal hyperoxic lung injury. Respir Res 2009;10:30.
[58] Parker TA, Abman SH. The pulmonary circulation in bronchopulmonary dysplasia. Semin Neonatol 2003;8(1):51–61.
[59] Baker CD, Abman SH, Mourani PM. Pulmonary Hypertension in Preterm Infants with Bronchopulmonary Dysplasia. Pediatr Allergy Immunol Pulmonol 2014;27(1):8–16.
[60] Aslam M, Baveja R, Liang OD, Fernandez-Gonzalez A, Lee C, Mitsialis SA, Kourembanas S. Bone marrow stromal cells attenuate lung injury in a murine model of neonatal chronic lung disease. Am J Respir Crit Care Med 2009;180(11):1122–30.
[61] Egashira K, Koyanagi M, Kitamoto S, Ni WH, Kataoka C, Morishita R, Kaneda Y, Akiyama C, Nishida KI, Sueishi K, Takeshita A. Anti-monocyte chemoattractant protein-1 gene therapy inhibits vascular remodeling in rats: blockade of MCP-1 activity after intramuscular transfer of a mutant gene inhibits vascular remodeling induced by chronic blockade of NO synthesis. FASEB J 2000;14(13):1974–8.
[62] Ikeda Y, Yonemitsu Y, Kataoka C, Kitamoto S, Yamaoka T, Nishida KI, Takeshita A, Egashira K, Sueishi K. Anti-monocyte chemoattractant protein-1 gene therapy attenuates pulmonary hypertension in rats. Am J Physiol-Heart C 2002;283(5):H2021–8.
[63] Thompson A, Bhandari V. Pulmonary Biomarkers of Bronchopulmonary Dysplasia. Biomark Insights 2008;3:361–73.
[64] Chang YS, Oh W, Choi SJ, Sung DK, Kim SY, Choi EY, Kang S, Jin HJ, Yang YS, Park WS. Human Umbilical Cord Blood-Derived Mesenchymal Stem Cells Attenuate Hyperoxia-Induced Lung Injury in Neonatal Rats. Cell Transplant 2009;18(8):869–86.
[65] Goodman RB, Strieter RM, Martin DP, Steinberg KP, Milberg JA, Maunder RJ, Kunkel SL, Walz A, Hudson LD, Martin TR. Inflammatory cytokines in patients with persistence of the acute respiratory distress syndrome. Am J Resp Crit Care 1996;154(3):602–11.
[66] Sutsko RP, Young KC, Ribeiro A, Torres E, Rodriguez M, Hehre D, Devia C, McNiece I, Suguihara C. Long-term reparative effects of mesenchymal stem cell therapy following neonatal hyperoxia-induced lung injury. Pediatr Res 2013;73(1):46–53.
[67] van Haaften T, Byrne R, Bonnet S, Rochefort GY, Akabutu J, Bouchentouf M, Rey-Parra GJ, Galipeau J, Haromy A, Eaton F, Chen M, Hashimoto K, Abley D, Korbutt G, Archer SL, Thebaud B. Airway delivery of mesenchymal stem cells prevents arrested alveolar growth in neonatal lung injury in rats. Am J Respir Crit Care Med 2009;180(11):1131–42.
[68] Fung ME, Thebaud B. Stem cell-based therapy for neonatal lung disease: it is in the juice. Pediatr Res 2014;75(1-1):2–7.
[69] de Paula S, Greggio S, Marinowic DR, Machado DC, DaCosta JC. The dose-response effect of acute intravenous transplantation of human umbilical cord blood cells on brain damage and spatial memory deficits in neonatal hypoxia-ischemia. Neuroscience 2012;210:431–41.
[70] Furlani D, Ugurlucan M, Ong L, Bieback K, Pittermann E, Westien I, Wang W, Yerebakan C, Li W, Gaebel R, Li RK, Vollmar B, Steinhoff G, Ma N. Is the intravascular administration of mesenchymal stem cells safe? Mesenchymal stem cells and intravital microscopy. Microvasc Res 2009;77(3):370–6.
[71] Chang YS, Choi SJ, Ahn SY, Sung DK, Sung SI, Yoo HS, Oh WI, Park WS. Timing of umbilical cord blood derived mesenchymal stem cells transplantation determines therapeutic efficacy in the neonatal hyperoxic lung injury. PLoS One 2013;8(1):e52419.
[72] Ortiz LA, Gambelli F, McBride C, Gaupp D, Baddoo M, Kaminski N, Phinney DG. Mesenchymal stem cell engraftment in lung is enhanced in response to bleomycin exposure and ameliorates its fibrotic effects. Proc Natl Acad Sci USA 2003;100(14):8407–11.
[73] Chang YS, Ahn SY, Yoo HS, Sung SI, Choi SJ, Oh WI, Park WS. Mesenchymal stem cells for bronchopulmonary dysplasia: phase 1 dose-escalation clinical trial. J Pediatr 2014;164(5):966–72. e6.
[74] Ahn SY, Chang YS, Kim JH, Sung SI, Park WS. Two-Year Follow-Up Outcomes of Premature Infants Enrolled in the Phase I Trial of Mesenchymal Stem Cells Transplantation for Bronchopulmonary Dysplasia. J Pediatr 2017;185:49–54. e2.
[75] Kumai Y, Ooboshi H, Takada J, Kamouchi M, Kitazono T, Egashira T, Ibayashi S, Iida M. Anti-monocyte chemoattractant protein-1 gene therapy protects against focal brain ischemia in hypertensive rats. J Cereb Blood Flow Metab 2004;24(12):1359–68.
[76] Yao Z, Keeney M, Lin TH, Pajarinen J, Barcay K, Waters H, Egashira K, Yang F, Goodman S. Mutant monocyte chemoattractant protein 1 protein attenuates migration of and inflammatory cytokine release by macrophages exposed to orthopedic implant wear particles. J Biomed Mater Res A 2014;102(9):3291–7.
[77] Koga M, Kai H, Egami K, Murohara T, Ikeda A, Yasuoka S, Egashira K, Matsuishi T, Kai M, Kataoka Y, Kuwano M, Imaizumi T. Mutant MCP-1 therapy inhibits tumor angiogenesis and growth of malignant melanoma in mice. Biochem Bioph Res Co 2008;365(2):279–84.